Size-dependent thermal stresses in the core–shell nanoparticles

Astefanoaei I†, Dumitru I, and Stancu Al

Faculty of Physics, "Alexandru Ioan Cuza" University of Iasi, 700506, Iasi, Romania

(Received 15 January 2013; revised manuscript received 5 April 2013)

The thermal stress in a magnetic core–shell nanoparticle during a thermal process is an important parameter to be known and controlled in the magnetization process of the core–shell system. In this paper we analyze the stress that appears in a core–shell nanoparticle subjected to a cooling process. The external surface temperature of the system, considered in equilibrium at room temperature, is instantly reduced to a target temperature. The thermal evolution of the system in time and the induced stress are studied using an analytical model based on a time-dependent heat conduction equation and a differential displacement equation in the formalism of elastic displacements. The source of internal stress is the difference in contraction between core and shell materials due to the temperature change. The thermal stress decreases in time and is minimized when the system reaches the thermal equilibrium. The radial and azimuthal stress components depend on system geometry, material properties, and initial and final temperatures. The magnitude of the stress changes the magnetic state of the core–shell system. For some materials, the values of the thermal stresses are larger than their specific elastic limits and the materials begin to deform plastically in the cooling process. The presence of the induced anisotropy due to the plastic deformation modifies the magnetic domain structure and the magnetic behavior of the system.

Keywords: thermal stresses, thermal equilibrium, core–shell particle

PACS: 81.40.Lm, 81.70.Pg, 65.80.−g, 46.25.Hf **DOI:** 10.1088/1674-1056/22/12/128102

1. Introduction

In the past years, the nanoparticles with core–shell structure have been intensively studied due to their biological and medical applications in magnetic separation and hyperthermia treatment.[1–4] Core–shell structures can also have magnetic properties for spintronics and recording medium applications.[5–8] Nanometric core–shell particles display peculiar magnetic and transport properties that are not present in the bulk materials.[6,7] Typically, these particles are ellipsoidal or spherical in shape and consist of a core (usually magnetic) surrounded by a concentric shell (magnetic or not).[9–12]

The behaviors of core–shell structures were intensively investigated in order to explain the magnetic properties in various thermal processes.[13–17] The analysis of induced thermal stresses provides information about the magnetic anisotropy, magnetic domains shape, switching mechanism,[17–19] etc. The analysis of thermodynamics in the thermal process is an important research topic in the nanoscale dimension.[20,21]

The goal of this paper is to study the thermal stresses in a magnetic core–shell nanoparticle during the cooling from the room temperature to a lower temperature. An analytical model is developed to predict the temperature profile and thermal stress in the core–shell system. This allows a direct computation of the thermal stress in the transitory process as well as at the thermal equilibrium using material and geometric parameters.

In the paper analyzed are the following contents: 1) thermal behavior of the system; 2) the thermal stress at the end of the cooling process when the system reaches the thermal equilibrium; 3) the effect of temperature decreasing speed of the external surface on the thermal stress evolution in the cooling process with consideration to a small cooling rate of the external surface necessary to maintain the thermal equilibrium at each moment of the cooling process.

The azimuthal and radial stresses depend on the radius of the metallic core and thickness of the shell, being negative due to the thermal contraction during the cooling process. The numerical results are evaluated for the following materials: iron, cobalt, and permalloy. For some core–shell dimensions the values of the thermal stresses induced by the cooling process are larger than their specific elastic limits.[22,23] Over this elastic limit the system is plastically deformed and a permanent magnetic anisotropy is induced. The presence of the induced anisotropy due to the plastic deformation modifies the magnetic domain structure and the magnetic behavior of the system.

2. Temperature distribution of the system

A system composed of a spherical particle surrounded by a shell is considered (Fig. 1). The spherical core has the radius R_1 and the shell thickness is $\delta R = R_2 - R_1$. The radius of the spherical system consisting of core and shell is R_2.

*Project supported by Romanian CNCS–UEFISCDI project IDEI-EXOTIC (Grant No. 185/25.10.2011).

†Corresponding author. E-mail: h.hasanabadi@shahroodut.ac.ir

© 2013 Chinese Physical Society and IOP Publishing Ltd

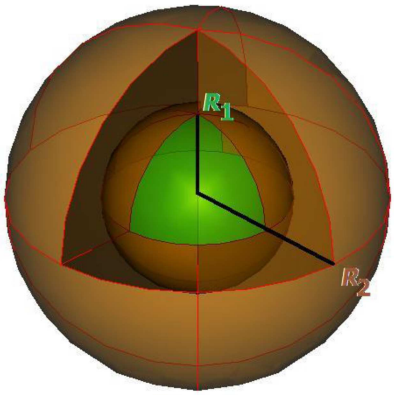


Fig. 1. (color online) Geometric configuration of the core–shell system. R_1 is the core radius and R_2 is the system radius.

2.1. Temperature distribution in core

The spatiotemporal temperature distribution $T_1(r,t) \equiv T_1$ of the core particle subjected to a cooling process, starting from the initial room temperature $T_{\rm in}$ to the lower target temperature $T_{\rm fin}$ is calculated. In the cooling process, the external surface of the system is maintained at temperature $T_{\rm fin}$. At all points in the system the temperature is the same $T_{\rm in}$ at the beginning of the cooling process $t = 0$. The amount of heat distributed in the shell volume $V_2 - V_1$ is expressed as:[24]

$$Q = \frac{-3k_1R_1R_2}{(R_2^3 - R_1^3)(R_2 - R_1)}(T_1(r,t) - T_{\rm fin}), \tag{1}$$

where k_1 is thermal conductivity of the core.

The temperature distribution in core is described by the time-dependent heat conduction equation (Fourier heat transport equation) as[24]

$$\rho_1 c_p \frac{\partial T_1}{\partial t} + \nabla \cdot (-k_1 \nabla T_1) = Q, \tag{2}$$

where Q is the heat received from shell, ρ_1 is the mass density of the core, and c_{p1} is the specific heat of the core.

The general solution of this equation has the following form:

$$T_1(x,\tau) = T_{\rm fin} + (T_{\rm in} - T_{\rm fin}) \sum_{j=1}^{\infty} A_j \left(\frac{\sin(\alpha_j x)}{xR_1} \right) {\rm e}^{-\beta_j^2 \tau}, \quad 0 < x < 1. \tag{3}$$

In this equation, the dimensionless variable $x = r/R_1$ is used. For $r = R_1$, $x = 1$. The dimensionless variable x becomes $x_1 = R_2/R_1$ for $r = R_2$. The parameter x_1 is a dimensionless thickness parameter. The values $\beta_j = \sqrt{\alpha_j^2 + bR_1^2/a}$ and $\alpha_j = m_j R_1$ $(j = 1, 2, \ldots)$ are the eigenvalues of the eigenfunctions $\sin(m_j r)$ and τ is the parameter given by the relation $\tau = at/R_1^2$. The constants a and b are $a = k_1/(\rho_1 c_p)$ and $b = 3x_1 a/[R_1^2(x_1^3 - 1)(x_1 - 1)]$. The orthogonality properties of the eigenfunctions yield the following coefficients

$$A_j = \frac{R_1 \int_0^1 x \sin(\alpha_j x)\,{\rm d}x}{\int_0^1 \sin^2(\alpha_j x)\,{\rm d}x}.$$

At the beginning of the cooling process, the temperature of central point is the initial temperature $T_{\rm in}$ and there are not radial temperature gradients, i.e.,

$$\begin{cases} T_1(x = 0, t = 0) = T_{\rm in}, \\ (\partial T_1/\partial x)|_{x=0} = 0. \end{cases} \tag{4}$$

The eigenvalues α_j will be obtained from the following boundary conditions at the core–shell interface.

2.2. Temperature distribution in shell

In the cooling process, the shell reaches instantly the target temperature and the transitory effects in the shell are not considered. Therefore, the general solution of the Fourier heat transport equation[24] for the shell is given in the following form:

$$T_2(x,\tau) = C_1(\tau) + \frac{C_2(\tau)}{xR_1}, \quad 1 < x < x_1. \tag{5}$$

The constants $C_1(\tau) = C_1$ and $C_2(\tau) = C_2$ depend only on parameter τ.

2.3. Boundary conditions on the spherical core–shell interface

In order to obtain the expressions of the core temperature $T_1(x,\tau)$ and the shell temperature $T_2(x,\tau)$ the following boundary conditions are considered.

(i) The heat flux is imposed to be continuous on core–shell interface $x = 1$

$$k_1(\partial T_1/\partial x)|_{x=1} = k_2(\partial T_2/\partial x)|_{x=1}, \tag{6}$$

where k_1 and k_2 are the coefficients of thermal conductivity of the core and of the shell respectively;

(ii) At the core–shell interface $(x = 1)$, the temperatures of the adjacent regions are considered to be the same, i.e.,

$$T_1(x = 1) = T_2(x = 1); \tag{7}$$

(iii) The temperature at the external surface of the shell is the target temperature $T_{\rm fin}$, i.e.,

$$T_2(x = x_1) = T_{\rm fin}. \tag{8}$$

Using these boundary conditions the following expressions for C_1 and C_2 are obtained as

$$C_1(\tau) = T_{\rm fin} - \frac{(T_{\rm in} - T_{\rm fin})}{R_1(x_1 - 1)} \sum_{j=1}^{\infty} A_j {\rm e}^{-\beta_j^2 \tau} \sin(\alpha_j), \tag{9}$$

$$C_2(\tau) = -k_1 k_2^{-1}(T_{\rm in} - T_{\rm fin}) \times \sum_{j=1}^{\infty} A_j {\rm e}^{-\beta_j^2 \tau}(\alpha_j \cos(\alpha_j) - \sin(\alpha_j)) \tag{10}$$

and the eigenvalues α_j ($j = 1,2,3,\ldots$), solutions of transcendent equation are obtained as

$$\sin(\alpha_j) = \left(\frac{p\alpha_j}{p-1}\right)\cos(\alpha_j), \tag{11}$$

where the parameter p is

$$p = \frac{k_1}{k_2}\left(1 - \frac{1}{x_1}\right).$$

Therefore, the spatiotemporal temperature distributions in the system are given by Eqs. (3), (5), (9), (10), and (11). The analytical expression of temperature is evaluated for a system composed of a cobalt core with radius $R_1 = 100$ nm and alumina shell thickness $\delta R = R_2 - R_1 = 20$ nm. The system considered initially to be in equilibrium at temperature $T_{\text{in}} = 300$ K is cooled by instant changing of external surface temperature to $T_{\text{fin}} = 3$ K. The constants $C_1(\tau)$ and $C_2(\tau)$ used in Eqs. (9) and (10) are calculated considering the following material parameters: $c_{p1} = 427$ J/kg·K, $k_1 = 100$ W/mK, $k_2 = 27$ W/mK, and $\rho_1 = 8836$ kg/m^3.[25] The thermal diffusivity $\alpha = k_1/(\rho \cdot c_{p1}) = 2.6 \cdot 10^{-5}$ m^2/s leads to the thermal time constant $\tau_c = R_1^2/\alpha = 4 \cdot 10^{-10}$ s which is larger than the thermal relaxation time $\tau_0 = 1.8 \cdot 10^{-13}$ s[25] of the cobalt material ($\tau_c \gg \tau_0$) as occur in macroscopic phenomena.[26–29]

For a smaller radius of the system, such as $R_1 = 10$ nm and $R_2 = 12$ nm, the thermal time constant τ_c becomes comparable to the thermal relaxation time τ_0 and non-Fourier heat conduction needs to be considered.[29] In this case, there exists a significant difference between the temperature value computed by a non-Fourier heat conduction equation and that obtained by a classical Fourier heat conduction equation.

The non-Fourier heat conduction can be approximated as Fourier heat conduction if the thermal time constant for thermal diffusion τ_c is much larger than the thermal relaxation time τ_0 corresponding to the non-Fourier heat conduction and implicitly to the thermal wave which exists on a small distance. The thermal wave can lead to different temperature profiles from that given by the classical Fourier equation. This interesting thermal behavior depends on the values of the size parameters (core radius and system radius).

For larger values of system radii $R_1 = 100$ nm and $R_2 = 120$ nm, the thermal time constant τ_c is larger than the thermal relaxation time τ_0. In this case, some small differences between the temperature value computed by the non-Fourier equation and that by the Fourier equation, are observed only on a distance around 20 nm. These temperature differences demonstrate that the thermal wave is existing and dominant on this short distance. Out of this distance there is no difference between the temperature values computed by the two equations. As a consequence, it is considered that the classical Fourier equation can be used to describe the temperature in the system with this dimension.

In order to determine the influence of the shell thickness on the temperature distribution the system geometry parameters are modified accordingly. The temperature distributions are computed for different shell thickness values and the same core radius. The time evolutions of the temperature at the core–shell interface at different shell thickness values are presented in Fig. 2(a). It is observed that the exponentially decreasing rate of the temperature is more important for smaller shell thickness. The presence of a large shell leads to a small decrease of the temperature in the core and consequently the time necessary to reach the thermal equilibrium is longer. The increase of the shell thickness isolates more the core by the external surface and the thermal equilibrium is obtained more slowly. Figure 2(b) shows the radial distributions of the temperature at the time moment $t = 1.9$ ns. As expected the temperature is maximal in the core center and decreases toward the external surface where the temperature is T_{fin}. The shell thickness influences the temperature distribution in the core; for a larger shell the core temperature and the difference in temperature between the center and interface are higher. The results presented in this figure show that by changing the size parameters of the system (core radius and alumina shell thickness), the cooling process can be controlled.

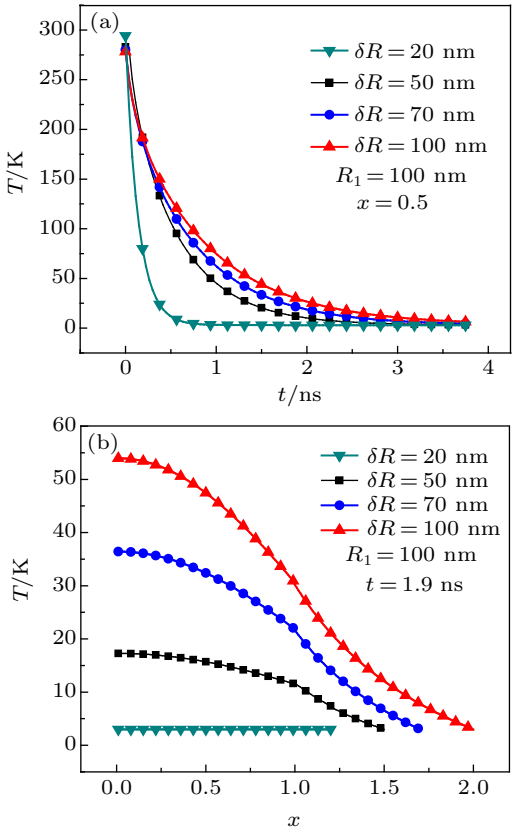


Fig. 2. (color online) (a) Time evolutions of the temperature at $x = 0.5$ in the core for different values of the thickness: $\delta R_1 = 20$ nm, $\delta R_2 = 50$ nm, $\delta R_3 = 70$ nm, $\delta R_3 = 100$ nm and (b) radial distributions of the temperature at the time moment $t = 1.9$ ns and different values of thickness.

The time evolutions of temperature for different core

materials (iron, cobalt, permalloy) are analyzed using the same alumina shell (Fig. 3). The material parameters are i) permalloy with $k_1 = 46.4$ W/mK, $c_{p1} = 430$ J/kg·K, and $\rho_1 = 8700$ Kg/m^3, ii) iron with $k_1 = 80.3$ W/mK, $c_{p1} = 460$ J/kg·K, and $\rho_1 = 7850$ Kg/m^3. In our evaluation these parameters are considered for bulk material. On the nanoscale the thermal characteristics of the materials are size-dependent[30] and this could be considered for accurately determining the structure behavior.

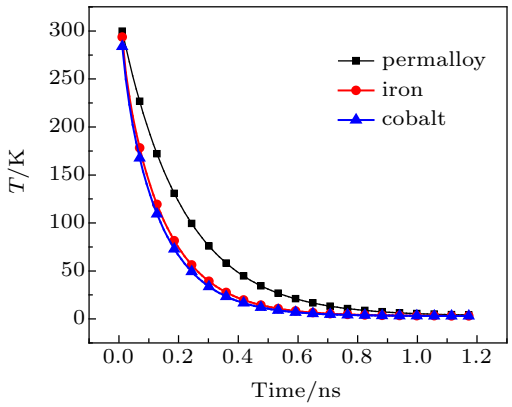


Fig. 3. (color online) Time evolutions of temperature in the core for different materials: permalloy, iron, and cobalt at point $x = 0.5$.

The core radius is $R_1 = 100$ nm and the shell thickness is $\delta R = R_2 - R_1 = 20$ nm. Due to the smaller values of thermal conductivity and specific heat capacity, the temperature decreasing rate is smaller for permalloy. However, the time necessary to reach the thermal equilibrium is almost the same for the considered materials (around 1 ns).

The cobalt particles have a thermal diffusivity $\alpha = k_1/(\rho \cdot c_{p1}) = 2.6 \times 10^{-5}$ m^2/s which is higher than the thermal diffusivity for iron: $\alpha = k_1/(\rho \cdot c_{p1}) = 2.2 \times 10^{-5}$ m^2/s or permaloy: $\alpha = k_1/(\rho \cdot c_{p1}) = 1.25 \times 10^{-5}$ m^2/s. The cobalt particle cools in a shorter time due to the high thermal diffusivity in comparison with those of iron and permalloy. The thermal equilibrium is reached quicker in the cobalt particles than in the permalloy particles.

3. Thermal stress induced in the core–shell particles

3.1. Thermal stress in the transient stage of temperature

The thermal stresses that appear in the cooling process of the system are computed using the spatiotemporal temperature distribution determined in Section 2. The radial temperature gradients lead to the occurring of some displacements both in the core (u_x^{core}) and in the shell (u_x^{shell}). These displacements satisfy the differential displacements equation.[30] Consequently, using the elastic formalism,[31] the thermal stress produced by the thermal gradient can be obtained. The analytical expressions of the thermal stress components are given by

$$\sigma_{rr}^{\text{core}}(x,\tau) = -\left(\frac{4\mu_1\alpha_1}{x^3}\right)\left(\frac{3\lambda_1+2\mu_1}{\lambda_1+2\mu_1}\right) \times \int_0^x x^2 T_1(x,\tau)\,\mathrm{d}x + (3\lambda_1+2\mu_1)C_3, \tag{12}$$

$$\sigma_{\theta\theta}^{\text{core}}(x,\tau) = \sigma_{\phi\phi}^{\text{core}}(x,\tau) = \left(\frac{2\mu_1\alpha_1}{x^3}\right)\left(\frac{3\lambda_1+2\mu_1}{\lambda_1+2\mu_1}\right)\int_0^x x^2 T_1(x,\tau)\,\mathrm{d}x + (3\lambda_1+2\mu_1)C_3 - 2\mu_1\left(\frac{3\lambda_1+2\mu_1}{\lambda_1+2\mu_1}\right)\alpha_1 T_1(x,\tau), \tag{13}$$

$$\sigma_{rr}^{\text{shell}}(x,t) = -\left(\frac{4\mu_2\alpha_2}{x^3}\right)\left(\frac{3\lambda_2+2\mu_2}{\lambda_2+2\mu_2}\right)\int_1^x x^2 T_2(x,\tau)\,\mathrm{d}x + (3\lambda_2+2\mu_2)C_1 - \frac{4\mu_2\overline{C}_2}{x^3}, \tag{14}$$

$$\sigma_{\theta\theta}^{\text{shell}}(x,t) = \sigma_{\phi\phi}^{\text{shell}}(x,t) = \left(\frac{2\mu_2\alpha_2}{x^3}\right)\left(\frac{3\lambda_2+2\mu_2}{\lambda_2+2\mu_2}\right)\int_1^x x^2 T_2(x,\tau)\,\mathrm{d}x + (3\lambda_2+2\mu_2)C_1 + \frac{2\mu_2\overline{C}_2}{x^3} - 2\mu_2\left(\frac{3\lambda_2+2\mu_2}{\lambda_2+2\mu_2}\right)\alpha_2 T_2(x,\tau), \tag{15}$$

where $T_1(x,\tau)$ and $T_2(x,\tau)$ are the spatiotemporal temperature distributions of the core and shell given by Eqs. (3) and (5) respectively. The C_1, $\overline{C}_2 = C_2/R_1^3$, and C_3 are the constants of integration.

In Eqs. (12)–(15) α_1 and α_2 are the thermal expansion coefficients for the core and shell respectively. The Lamè elastic constants λ_1, λ_2, μ_1, and μ_2 are related to E_1, E_2, υ_1, and υ_2 as follows:

$$\lambda_1 = \frac{\upsilon_1 E_1}{(1+\upsilon_1)(1-2\upsilon_1)}, \quad \lambda_2 = \frac{\upsilon_2 E_2}{(1+\upsilon_2)(1-2\upsilon_2)},$$
$$\mu_1 = \frac{E_1}{2(1+\upsilon_1)}, \quad \mu_2 = \frac{E_2}{2(1+\upsilon_2)},$$
$$3\lambda_1+2\mu_1 = 3k_{\text{core}}, \quad 3\lambda_2+2\mu_2 = 3k_{\text{shell}},$$
$$E_1 = \frac{(3\lambda_1+2\mu_1)\mu_1}{(\lambda_1+\mu_1)}, \quad E_2 = \frac{(3\lambda_2+2\mu_2)\mu_2}{(\lambda_2+\mu_2)},$$
$$\upsilon_1 = \frac{\lambda_1}{2(\lambda_1+\mu_1)}, \quad \upsilon_2 = \frac{\lambda_2}{2(\lambda_2+\mu_2)},$$

where E_1 and E_2 are the Young's moduli, υ_1 and υ_2 are the Poisson's coefficients, and k_{core} and k_{shell} are the bulk moduli for the core and shell respectively.[32,33] The strains due to the thermal contraction in the core and shell are $\varepsilon_{\text{core}} = \alpha_1 \Delta T$ and $\varepsilon_{\text{shell}} = \alpha_2 \Delta T$ respectively, where $\Delta T = T_1 - T_{\text{fin}}$ is the temperature variation at the core–shell interface. The resultant strain at core–shell interface is

$$\varepsilon(x=1,\tau) = \varepsilon_{\text{core}} - \varepsilon_{\text{shell}} = (\alpha_1 - \alpha_2)(T_1(x=1,\tau) - T_{\text{fin}}).$$

The numerical values of the constants: $C_1, \overline{C}_2$, and C_3 are determined by imposing the boundary conditions at material interfaces, taking into account the different mechanical behav-

iors of the materials in contact. The following conditions are imposed on the core–shell interfaces:

(I) the strains appear in the cooling process which result from the difference between in thermal expansion coefficients between the core and shell:

$$u_x^{\text{core}}(x=1,\tau)-u_x^{\text{shell}}(x=1,\tau)=\varepsilon(x=1,\tau)R_1; \quad (16)$$

(II) the equilibrium condition for stresses on the core–shell interface:

$$\sigma_{rr}^{\text{core}}(x=1,\tau)=\sigma_{rr}^{\text{shell}}(x=1,\tau); \quad (17)$$

(III) the nullifying stress condition on the external surface ($r=R_2$) of the system:

$$\sigma_{rr}^{\text{shell}}(x=x_1,\tau)=0, \ \ (x_1=R_2/R_1). \quad (18)$$

The explicit forms of the thermal stresses and radial displacements induced in the core and shell are obtained by substituting the constants $C_1, \overline{C}_2, C_3$ into Eqs. (12)–(15).

These thermal stresses that appear in the core and shell are due to both the thermal gradients and the constraints produced on the alumina membrane by its cooling that results in the difference in the thermal expansion coefficient between the two materials in contact.

3.2. Thermal stress at thermal equilibrium

At the end of the cooling process ($t\to\infty$) the system reaches thermal equilibrium. The particular expressions of the thermal stresses at thermal equilibrium are

$$\sigma_{rr-eq}^{\text{core}}(x_1,T_{\text{in}},T_{\text{fin}})=(3\lambda_1+2\mu_1)\Big(\frac{-4\mu_1\alpha_1(T_{\text{in}}-T_{\text{fin}})}{3(\lambda_1+2\mu_1)}+C_3'\Big), \quad (19)$$

$$\sigma_{rr-eq}^{\text{shell}}(x,x_1,T_{\text{in}},T_{\text{fin}})=(3\lambda_2+2\mu_2)\Big(\frac{-4\mu_2\alpha_2(T_{\text{in}}-T_{\text{fin}})}{3(\lambda_2+2\mu_2)}\frac{x^3-1}{x^3}+C_1'-\frac{a_1C_2'}{x^3}\Big), \quad (20)$$

where the constants C_1', C_2', and C_3' are given by the following expressions:

$$C_1'=-\Big(\frac{x_1^3(-a_1a_4-a_2a_4)+a_3a_1+a_1a_4+a_2a_4-a_1a_2a_5}{(a_2+a_1)x_1^3+a_1(a_2-1)}\Big),$$

$$C_2'=-\Big(\frac{x_1^3(a_2a_4-a_2a_5+a_3-a_4)+a_4-a_2a_4}{(a_2+a_1)x_1^3+a_1(a_2-1)}\Big),$$

$$C_3'=\Big(\frac{x_1^3(-a_5a_1+a_4+a_1a_4-a_3)-a_3a_1+a_5a_1-a_4-a_1a_4}{(a_2+a_1)x_1^3+a_1(a_2-1)}\Big).$$

The coefficients a_1, a_2, a_3, a_4, and a_5 are

$$a_1=\frac{4\mu_2}{3\lambda_2+2\mu_2}, \quad a_2=\frac{3\lambda_1+2\mu_1}{3\lambda_2+2\mu_2},$$

$$a_3=\Big(\frac{-4\mu_1\alpha_1}{3(3\lambda_2+2\mu_2)}\Big)\Big(\frac{3\lambda_1+2\mu_1}{\lambda_1+2\mu_1}\Big)\Delta T,$$

$$a_4=\Big(\frac{4\mu_2\alpha_2}{3(\lambda_2+2\mu_2)}\Big)\Delta T, \quad \text{and} \quad a_5=\frac{\alpha_1}{3}\Big(\frac{3\lambda_1+2\mu_1}{\lambda_1+2\mu_1}\Big)\Delta T.$$

The values of the thermal stresses at equilibrium in the core–shell structure during cooling can be simply computed by substituting the material parameters into Eqs. (19) and (20). The linear proportionality between thermal stress and the difference between initial and target temperatures can be directly observed. The radial thermal stresses in the core–shell particle at thermal equilibrium depend on T_{in}, T_{fin}, and dimensionless parameter x_1.

3.3. Thermal stresses for different cooling rates

In the following, it is considered that the cooling of the external surface to the target temperature T_{fin} is not an instant process as described before, but it is a linear cooling process determined by a finite cooling time t_{f} and a cooling rate $v_{\text{f}}=(T_{\text{in}}-T_{\text{fin}})/t_{\text{f}}$. The temperature of the system's external surface is expressed as

$$T_{\text{ext}}=\Big(\frac{T_{\text{fin}}-T_{\text{in}}}{t_{\text{f}}}\Big)t+T_{\text{in}}. \quad (21)$$

In this approach, the system evolves from room temperature T_{in} to the target temperature, T_{fin}, passing through different thermal equilibrium states. The thermal stresses are computed from Eqs. (19) and (20) by using the expression of external temperature (21). The cooling rate of the external surface is a supplementary parameter that characterizes the evolution of the thermal stress in the core–shell system.

4. Results and discussion

The effects of the shell thickness on stress distribution are studied by changing the system geometry parameters. The stress distributions are computed for different shell thickness values and the same core radius. The temporal evolutions of the stress on the core–shell interface at different shell thickness values are presented in Fig. 4(a). It is observed that the values of radial stress increase with time increasing, the increase rate being higher for a smaller shell thickness. The system with the smaller thickness reaches the mechanical equilibrium faster, which is similar to the thermal behavior.

Figure 4(b) shows the radial stress distributions at a time moment $t=1.9$ ns. The radial stress reaches a maximum value at the core center and decreases toward the external surface where the stress is zero. The maximum value of stress is proportional to shell thickness.

The temporal evolutions of thermal stresses are analyzed for different core materials (iron, cobalt, permalloy) using the same alumina shell (Fig. 5). The elastic material parameters used are as follows: for permalloy $E_1=225$ GPa, $\nu_1=0.29$, and $\alpha_1=12.9\times10^{-6}$ K^{-1}; for iron, $E_1=211$ GPa, $\nu_1=0.30$, and $\alpha_1=11.8\times10^{-6}$ K^{-1}.

It is observed that the stress decreasing rate is smaller for permalloy, which is related to the temperature decreasing rate.

The greatest stress that can be applied without producing a plastic (permanent) deformation is called the elastic limit of the material. If the sample is loaded beyond the elastic limit only the elastic strain can be recovered but the plastic strain is permanent. We are concerned only with those materials in which the Hooke's Law is valid, the stress is directly proportional to strain but independent of the rate of strain or past history. Over the elastic limit the elastic linear formalism cannot be used but gives an extrapolated value of the real thermal stress.

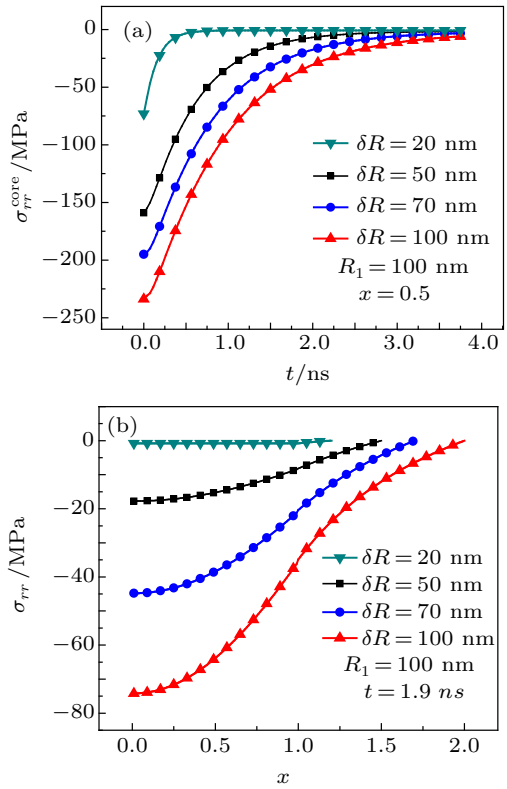


Fig. 4. (color online) (a) The time evolutions of the radial stress at $x = 0.5$ for thickness values of $\delta R = 20$ nm, 50 nm, 70 nm, and 100 nm, and (b) the radial distribution of the radial stresses at the time moment $t = 1.9$ ns and for thickness values of $\delta R = 20$ nm, 50 nm, 70 nm, and 100 nm. The radius of the core is $R_1 = 100$ nm.

It is observed from Fig. 5 that for iron and permalloy the elastic limits (120 MPa for iron and 100 MPa for permalloy) are exceeded in the cooling process. Beyond the elastic limit a plastic deformation of the core magnetic material is induced and the magnetic properties are irreversibly changed. A strain-hardening induced anisotropy is then observed. Supposing that the system is heated again to the initial temperature, after a forced cooling process in which the elastic limit is reached, the magnetic states will be different from the initial one. Therefore, the thermal process induces the irreversibility in the magnetic behavior.

According to a very simple discussion, supposing that the thermal stress σ (Nm ~ 2) acts on the ferromagnetic particle core and λ is the isotropic magnetostriction coefficient, the magnetoelastic energy is expressed as $E_\sigma = -(3/2)\lambda\sigma\cos^2\phi$ where ϕ is the angle of the magnetization with respect to the axis of stress.[26–28] As expressed in this form, the magnetoelastic energy is a kind of uniaxial magnetic anisotropy. The maximum value of the magnetoelastic energy will be $E_\sigma = -(3/2)\lambda\sigma$ if no radial variation of the thermal stresses is considered. Therefore the observed magneto-crystalline energies for different materials are compared with the corresponding values of the magneto-elastic energy.

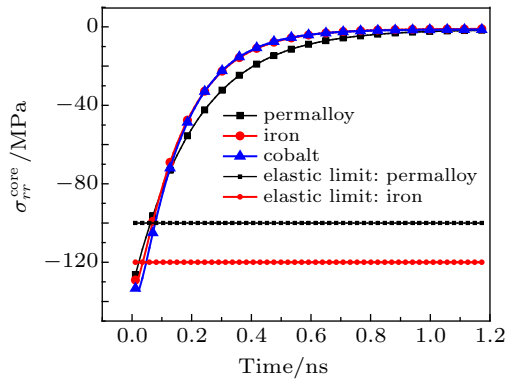


Fig. 5. (color online) Time evolutions of the radial stress in the core for different materials.

For Fe, the elastic limit is about 120 MPa, therefore the magneto-elastic energy is limited to about 104 erg/cc (1 erg $= 10^{-7}$ J).

This comparison was made in several papers previously by using the elastic limit of stress as the maximum value of stress possible in the core material and the estimated magneto-elastic energy was much smaller than the magneto-crystalline anisotropy energy.[15,34–39] Therefore the real value of magneto-elastic energy is greater than that computed by using the elastic limit, which is underestimated and smaller than that induced by magneto-crystalline or surface anisotropy.

In the following, the behavior of the radial stress of the core–shell particle at thermal equilibrium is analyzed. At the thermal equilibrium, there is no thermal gradient in the system.

Figure 6 shows the radial thermal stress distributions in the cross section of the system at the end of the cooling process for different values of the alumina thickness, with the core radius R_1 fixed. At the thermal equilibrium when the system reaches the $T_{\rm fin}$ temperature, the radial stress in the core has a negative constant value, its magnitude depends on the alumina thickness and temperature difference $(T_{\rm in} - T_{\rm fin})$. The radial stress increases with the increase of shell thickness. An explicit dependence of radial stress as a function of thickness parameter x_1 is presented in Fig. 7. The value of the thermal stress at equilibrium can be reduced by choosing a specific shell thickness. If the shell thickness is large enough $\delta R = R_1(x_1 - 1) > 4R_1$ the core radial stress becomes shell

thickness-independent.

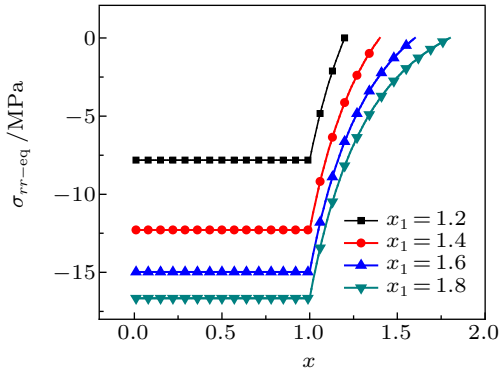


Fig. 6. (color online) Radial dependences of stresses in equilibrium for different values of shell parameter x_1 with t. The radius of the core being $R_1 = 100$ nm.

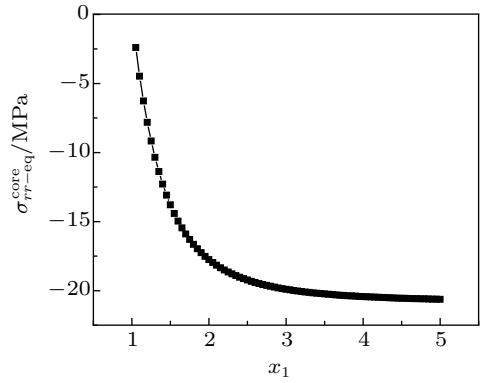


Fig. 7. Dependence of the radial stress on parameter (x_1).

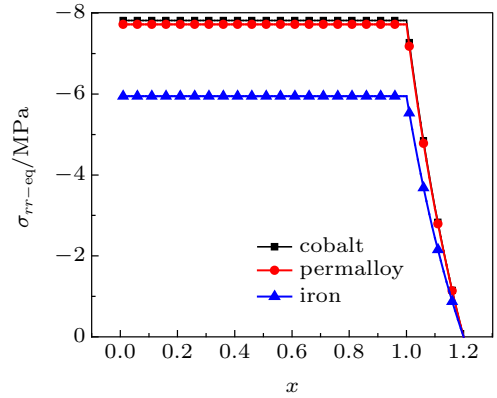


Fig. 8. (color online) Radial dependences of thermal stress at equilibrium for different core materials.

Figure 8 shows the radial thermal stresses in the cross section of the system at the thermal equilibrium for different core materials: cobalt, permalloy, and iron. The values of the thermal stresses are bigger for the permalloy core. The differences in radial stresses among materials are mainly due to their Young's moduli.

Figure 9 shows the values of the radial stresses in the cobalt core–shell system at thermal equilibrium for different cooling rates of the external surface. The values of the thermal stresses induced in the core are smaller for smaller values of cooling rate. It is observed that the elastic limit of core material is exceeded for some high cooling rates. In order to prevent exceeding this limit a small cooling rate is required. This implies more slowly cooling the external system surface. On the contrary, if a plastic deformation of the system is desired, a high cooling rate is necessary. Therefore, the cooling rate can be used to control the thermal stress induced in the system.

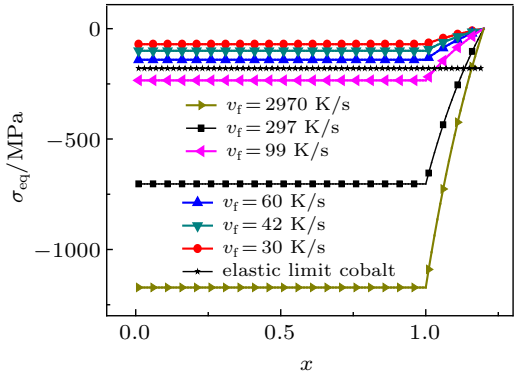


Fig. 9. (color online) Radial dependences of thermal stress for different cooling rates of the core–shell external surface.

5. Conclusions

In this paper we describe the thermal stresses which are induced in a core–shell system in a cooling process from an initial temperature to a target temperature. Using an analytical model we compute the temperature and stress in the case of a particular system composed of a cobalt core and an alumina shell, subjected to a cooling process starting from room temperature to 3 K. The center of the core reaches the final temperature in a time of around 1 ns. The magnitude order of the induced stresses is MPa. As a common feature, one can observe that all stresses tend toward their saturation values, corresponding to the thermal equilibrium at the target temperature. At the end of the cooling process, the values of the radial stresses are constant in the core.

For some core–shell materials and geometry parameters the values of the thermal stress induced by the cooling process are larger than their specific elastic limits. Over this elastic limit the system is plastically deformed and a permanent magnetic anisotropy is induced. The presence of the induced anisotropy due to the plastic deformation modifies the magnetic domain structure and the magnetic behavior of the system. Moreover we investigate the effects of the cooling rate on the thermal stress evolution of the system. A high cooling rate induces high stress in the core material. By modifying the cooling rate the thermal stress can be adjusted in order to exceed or prevent exceeding the elastic limit.

We also optimize the cooling rate which is an important step to control the thermal stress and to understand its influence on the magnetic behavior of the core–shell system.

The results presented in this paper show that by changing the values of the size parameters of the system (radius and

shell thickness) one can control the induced thermal stresses (radial and azimuthal thermal stresses) that appear in the system due to the forced cooling process. The results obtained in this paper are significant in technological applications, such as heat-assisted magnetic recording.

References

[1] Tartaj P, Morales M, Verdaguer S, Gonzalez-Carreno T and Serna C J 2003 *J. Phys. D: Appl. Phys.* **36** R182

[2] Duan H L, Karihaloo B L, Wang J and Yi X 2006 *Nanotechnology* **17** 3380

[3] Hood J D, Bednarski M, Frausto R, Guccione S, Reisfeld R A, Xiang R and Cheresh D A 2002 *Science* **296** 2404

[4] Batlle X and Labarta A 2002 *J. Phys. D: Appl. Phys.* **35** R15

[5] Meiklejohn W H and Bean C P 1957 *Phys. Rev. B* **105** 904

[6] Takano K, Kodama R H, Berkowitz A E, Cao W and Thomas G 1997 *Phys. Rev. Lett.* **79** 1130

[7] Martınez B, Obradors X, Balcells L, Rouanet A and Monty C 1998 *Phys. Rev. Lett.* **80** 181

[8] Bianco L, Hernando A, Multigner M, Prados C, Sanchez-Lopez J C, Fernandez A, Conde C F and Conde A 1998 *J. Appl. Phys.* **84** 2189

[9] Duan H L, Karihaloo B L, Wang J and Yi X 2006 *Nanotechnology* **17** 3380

[10] Wiggins J, Carpenter E E and O'Connor C J 2000 *J. Appl. Phys.* **87** 5651

[11] Abe M and Suwa T 2004 *Phys. Rev. B* **70** 235103

[12] Ammar M, Mazaleyrat F, Bonnet J P, Audebert P, Brosseau A, Wang G and Champion Y 2007 *Nanotechnology* **18** 285606

[13] Chen C, Kitakami O and Shimada Y 1998 *J. Appl. Phys.* **84** 2184

[14] Gangopadhyay S G C, Hadjipanayis B D, Sorensen C M, Klabunde K J, Papaefthymiou V and Kostikas A 1992 *Phys. Rev. B* **45** 9778

[15] Barandiaran J M, Gutierrez J and Garcia-Arribas A 2011 *Phys. Status Solidi A* **208** 1

[16] Colin J 2010 *Phys. Rev. B* **82** 054118

[17] Silva E L, Nunes W C, Knobel M, Denardin J C, Zanchet D, Pirota K, Navas D and Vázquez M 2006 *Physica B* **384** 22

[18] Astefanoaei I, Dumitru I, Diaconu A, Spinu L and Stancu Al 2008 *J. Appl. Phys.* **103** 07D930

[19] Astefanoaei I, Stancu Al and Chiriac H 2007 *J. Magn. Magn. Mater.* **316** E276

[20] Qin W P, Qin G S, Zhang J S, Wu C F, Wang J W and Du G T 2001 *Acta Phys. Sin.* **50** 1467 (in Chinese)

[21] Zhang A L, He Z Y and Su L R 2007 *Chin. Phys.* **16** 3747

[22] Howatson A M, Lund P G and Todd J D 2005 *Engineering Tables and Data* p. 41

[23] Dieter G E 1988 *Mechanical Metallurgy* (UK: McGraw-Hill) p. 36

[24] Schneider P J 1955 *Conduction Heat Transfer* (Cambridge: Addison Wesley Publishing Company Inc.) p. 18

[25] Singh J and Tomar S K 2011 *Int. J. Eng.* (Science and Technology) **3** 34

[26] Marin E 2010 *Lat. Am. J. Phys. Educ.* **4** 1

[27] Voz S 2007 *Topics in Applied Physics* (Paris: Springer) p. 1–13

[28] Wolf E L 2004 *Nanophysics and Nanotechnology: An Introduction to Modern Concepts in Nanoscience* (Weinheim: Wiley-VCH) p. 145

[29] Wang M, Yang N and Guo Z 2011 *J. Appl. Phys.* **110** 064310

[30] Gu X K and Yang B C 2007 *Chin. Phys.* **16** 3777

[31] Bosley B A and Weiner J H 1960 *Theory of Thermal Stresses* (New York: Wiley) p. 34

[32] Lekhnitskii S G 1977 *Theory of Elasticity of an Anisotropic Body* (Moscow: Mir Moscow Publishing Company Inc.) p. 48

[33] Landau L and Lifchitz E 1990 *Théorie de l'elasticité* (Moscow: Mir Moscow Publishing Company Inc.) p. 120

[34] Chikazumi S 1997 *Physics of Ferromagnetism* (Oxford: Clarendon Oxford Publishing Company Inc.) p. 377

[35] Williamson A J and Zunger A 1999 *Phys. Rev. B* **59** 15819

[36] Abe M, Kuroda J and Matsumoto M 2002 *J. Appl. Phys.* **91** 7373

[37] Abe M and Suwa T 2004 *Phys. Rev. B* **70** 23510

[38] Nielsen O V, Barandiaran J M, Hernando A and Madurga V 1985 *J. Magn. Magn. Mater.* **49** 124

[39] Barandiaran J M, Hernando A and Nielsen O V 1985 *J. Magn. Magn. Mater.* **46** 317